JOURNAL OF GEOPHYSICAL RESEARCH, VOL. 112, D13115, doi:10.1029/2006JD007939, 2007

Testing sprite initiation theory using lightning measurements and modeled electromagnetic fields

W. Hu,[1] S. A. Cummer,[1] and W. A. Lyons[2]

Received 20 August 2006; revised 5 March 2007; accepted 3 April 2007; published 10 July 2007.

[1] Previous research has shown that the statistical measurements of charge moment changes in sprite-producing lightning are in general agreement with the predictions based on the conventional breakdown theory for sprite initiation in the mesosphere. Measurements have progressed to the point where a detailed, event-level quantitative comparison between the measurements and predictions could more rigorously test the existing theories by estimating the electric fields above the thunderstorm clouds responsible for sprite initiation. We selected for this analysis a set of sprite events from the summer of 2004 whose initiation times are well bounded. Then we measured the current moments and charge moment changes of the parent lightning discharges using the radiated electromagnetic fields recorded by our extremely low frequency/ultra low frequency lightning remote sensing systems. The measured current moments were then used as the input of a two-dimensional cylindrical full-wave finite-difference time-domain model for lightning-generated electromagnetic field simulations. We compared the simulated mesospheric electric fields to the threshold electric field for conventional breakdown to see whether, according to theory, conventional breakdown (and thus a sprite) would be initiated by that electric field and at what altitude. By analyzing sprites that are both short and long delayed from the source lightning strokes, we compared measurements and theory across a wide range of timescales. The results show that for bright, short-delayed sprites, the measurement-inferred mesospheric electric field agrees within 20% with the threshold electric field for conventional breakdown. However, for long delayed sprite events and dimmer sprites, the measurement-inferred mesospheric electric field for sprite initiation is somewhat below the threshold for conventional breakdown.

Citation: Hu, W., S. A. Cummer, and W. A. Lyons (2007), Testing sprite initiation theory using lightning measurements and modeled electromagnetic fields, *J. Geophys. Res.*, *112*, D13115, doi:10.1029/2006JD007939.

1. Introduction

[2] Several theories have been developed to explain the mechanism of sprite initiation. According to conventional breakdown (CB) theory [*Pasko et al.*, 1997a, and references cited therein], the rapid charge transfer from the cloud to ground generates sustained intense quasi-electrostatic (QE) fields at the mesospheric altitude, which heat and ionize the background medium until a sprite is initiated in the form of a self-propagating streamer [*Pasko et al.*, 1998]. This QE theory combined with the streamer developing model [*Pasko et al.*, 1998; *Raizer et al.*, 1998] can explain the fine spatial structure of sprites [*Gerken et al.*, 2000]. The magnitude of the quasi-electrostatic field at high altitudes is basically proportional to the charge moment change during the lightning discharge. Another theory explaining sprite initiation is the runaway breakdown model [*Bell et al.*, 1995; *Roussel-Dupré and Gurevich*, 1996; *Taranenko and Roussel-Dupre*, 1996; *Lehtinen et al.*, 1997]. According to the runaway theory, preexisting high-energy electrons are heated by the same QE field, leading to the formation of a electron beam. The collisions between this electron beam and the air molecules result in optical emission. In addition to these primary mechanisms, it has been suggested that secondary factors could play a role in sprite initiation, including meteoritic dust [*Zabotin and Wright*, 2001] or neutral density depletions produced by atmospheric gravity waves [*Pasko et al.*, 1997b].

[3] Most previous research work on experimental testing of sprite initiation theory has focused on measuring the lightning charge moment change required for sprite generation. *Cummer and Inan* [1997] found the charge moment change for sprite producing lightning discharges varies from 25 to 3250 C km during the first 5 ms of the stroke, but these data were not analyzed in the context of the widely variable lightning-to-sprite initiation delays that are now well known. *Bell et al.* [1998] examined 17 sprites on a single day and deduced the total charge moment changes of

[1]Department of Electrical and Computer Engineering, Duke University, North Carolina, USA.
[2]Forensic Meteorology Associates, Research, Fort Collins, Colorado, USA.

0148-0227/07/2006JD007939$09.00

the parent lightning discharges. *Cummer and Stanley* [1999] calculated the charge moment change at the time of sprite initiation in their high-speed optical sprite observation. *Hu et al.* [2002] reported a careful statistical analysis of 76 sprites with well-defined initiation times and showed that a charge moment change between 600 and 1000 C km was sufficient to initiate a sprite. In an analysis of the impulse charge moment change in lightning discharges that did and did not produce sprites in multiple sprite-producing storms, *Cummer and Lyons* [2005] found that impulse charge moment changes of approximately 500 C km were required to initiate short-delayed sprites.

[4] These past measurements are generally consistent with CB theory, which predicts a charge moment change threshold of hundreds of Coulomb kilometers to produce breakdown [*Pasko et al.*, 1997a], although the precise value depends on the ambient conditions. Although the runaway breakdown electric field threshold is approximately 10 times smaller than the conventional breakdown threshold, the runaway model requires above-threshold electric fields over a large altitude extent in order to produce a beam capable of generating substantial optical emissions. Individual models vary somewhat in the precise charge moment change required, but they generally predict charge moment changes of several thousand Coulomb kilometers [*Yukhimuk et al.*, 1999; *Lehtinen et al.*, 2001]. However, the quantitative degree to which theory and observation agree has not been carefully investigated.

[5] These previous efforts in quantitative charge moment change measurements of sprite producing lightning have attempted to find the relation between charge moment changes and sprite generation. In this work, we took the next step through measurements and analysis conducted at the event level, where the quantitative comparison between the optical observation, model-predicted mesospheric electric field waveforms, and conventional breakdown threshold can rigorously test CB theory of sprite initiation. Instead of using an arbitrary charge transfer to represent the source, in this work the measured lightning discharge current waveforms obtained using our extremely low frequency (ELF)/ultra low frequency (ULF) remote sensing system were used as the source of the numerical model. Furthermore, a horizontal source geometry was included in the numerical model. Different ionosphere profiles were used to estimate the uncertainty of the simulation results caused by ionosphere variation. Nonlinear processes, such as heating and ionization, were considered carefully in the model to ensure the accuracy of the near-field simulation results. The idea is to include all currently understood effects so that model-data comparison is as realistic and precise as possible. *Thomas et al.* [2005] also predicted the high-altitude electric fields using the low-altitude electric fields obtained by the balloon measurements and a quasi-electrostatic field model [*Pasko et al.*, 1997a]. However, their simulation results lack high-frequency components because of the frequency band limitation of their numerical model; thus, the simulated high electric fields may not be right on short timescales. In addition, there were no sprites confirmed for the positive lightning discharges they studied.

[6] In this work, we selected a set of sprites that occurred in the summer of 2004 whose initiation times are well bounded, which means the uncertainty of the sprite initiation time window is short (see [*Hu et al.*, 2002] for the definition of the sprite initiation time window). Using the measured sferics (electromagnetic waves radiated by lightning discharges and propagating in the Earth-ionosphere waveguide) radiated by the positive lightning discharges producing these sprites, we predicted the high altitude electric field waveforms generated by the corresponding lightning discharges. Then, we analyzed a specific subset of these sprites (short-delayed sprites associated with sprite currents) whose initiation times can be determined accurately. By comparing the modeled quasi-electrostatic field at various altitudes with the theoretical electric field threshold for conventional breakdown, we are able to test CB theory on this specific class of sprites quantitatively. After that, we tested the CB theory on other general sprites (short-delayed sprites without sprite current and long-delayed sprites) in an effort to determine whether CB theory could explain the observation.

2. Testing Methods and Procedures

[7] Figure 1 shows a block diagram of the analysis procedure. The optical observation data were obtained from Yucca Ridge Field Station, Colorado, and the corresponding ELF/ULF sferics radiated by the causative lightning discharge currents were collected by our ELF/ULF lightning remote sensing system located at Duke University.

[8] The first step of this work was to inversely derive the lightning discharge current moment (the product of the electric current and the discharge channel length) waveforms from the distant magnetic fields. We followed the approach developed by *Cummer and Inan* [2000]. Since these lightning discharge locations are usually thousands kilometers away from the ELF/ULF receiver, the Earth-ionosphere waveguide can be regarded as a linear, time-invariant system [*Cummer and Inan*, 2000]. The input of this linear system is the lightning discharge current and the output is the sferic data recorded by our ELF/ULF remote sensing system. Thus, by correctly modeling the impulse response of the whole linear time-invariant system, we can inversely measure the input (lightning discharge current moment waveforms) by implementing the deconvolution of the impulse response and the system output (the sferic waveforms recorded by the remote sensing system). The impulse response can be calculated theoretically by using an finite-difference time-domain (FDTD) model [*Hu and Cummer*, 2006] or the mode theory model [*Cummer and Inan*, 2000] assuming a reasonable ionosphere profile. However, in this work, we adopted another method for the impulse response modeling. Because usually negative lightning discharges are more impulsive than positive lightning discharges, the averaging of many individual sferics radiated by negative lightning discharges at the same location and within a narrow time window can be regarded as the system impulse response of the Earth-ionosphere waveguide. Our analysis procedure includes 1 kHz low-pass filtering the recorded signals to simplify the deconvolution. This implies that any lightning stroke significantly shorter than approximately 1 ms appears impulsive in this bandwidth, a condition that most negative lightning strokes meet. We then scaled this averaged negative sferic waveform to the absolute units by a comparison with the mode theory predictions. The system impulse response derived in this

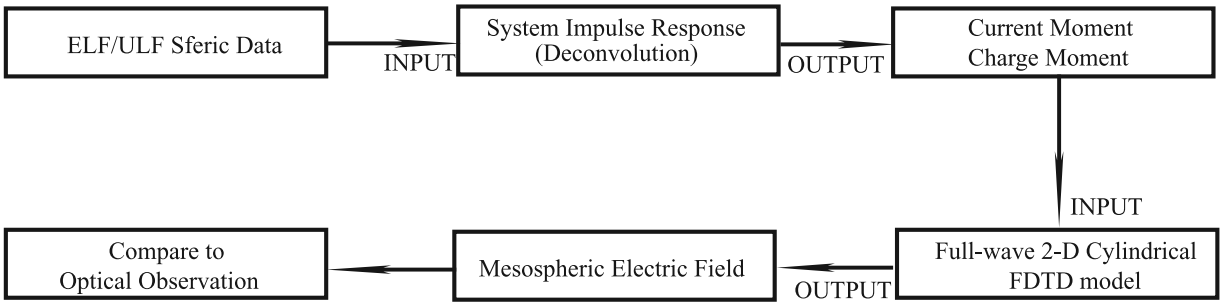

Figure 1. The QE sprite initiation theory testing methods and procedures.

way more precisely matches the true propagation impulse response. This results in greater reliability in the small details of the extracted current moment waveform, which are important for this study. Then, using the sferic waveforms of the sprite-producing lightning discharges, we are able to derive the corresponding current moment waveforms and the charge moment changes using a deconvolution approach [*Cummer and Inan*, 2000].

[9] The second step was to calculate the mesospheric electric field waveforms above the thunderstorms right after sprite-producing lightning discharges. To achieve this goal, the remotely measured current moment waveforms in the first step were used as the input to a full-wave two-dimensional cylindrical FDTD model developed for lightning-generated electromagnetic wave propagation in the ionosphere [*Hu and Cummer*, 2006]. Because this FDTD model is capable of simulating high-altitude electromagnetic fields produced by lightning discharges, we can realistically predict the mesospheric electric fields produced by sprite-producing lightning discharges.

[10] Finally, we compared the modeled mesospheric electric fields to the optical observation results and the conventional breakdown thresholds to determine the degree of agreement between CB theory and measurements. Specifically, we examine where and when CB theory predicts sprite initiation and compare this to the sprite observations.

3. Numerical Model

3.1. FDTD Model for Lightning-Generated Electromagnetic Wave Propagation

[11] The two-dimensional cylindrical full-wave FDTD model adopted in this work to predict high-altitude electromagnetic fields was originally developed for simulations of lightning-generated electromagnetic wave propagation in the ionosphere [*Hu and Cummer*, 2006]. This model removes some of the assumptions made in other existing models [*Ma et al.*, 1998; *Cummer*, 2000] addressing similar problems and treats the ionosphere as true cold plasma. The governing equations are shown in equations (1), (2), and (3):

$$\nabla \times \bar{E} = -\mu_0 \frac{\partial \bar{H}}{\partial t}, \tag{1}$$

$$\nabla \times \bar{H} = \varepsilon_0 \frac{\partial \bar{E}}{\partial t} + \bar{J}_{\text{tot}}, \tag{2}$$

$$\frac{\partial \bar{J}_n}{\partial t} + \nu_n \bar{J}_n = \frac{q_n}{|q_n|} \omega_{Bn} \left(\bar{J}_n \times \bar{b}_E\right) + \varepsilon_0 \omega_{pn}^2 \bar{E}, \tag{3}$$

where n denotes the different species of charged particles (electrons, positive ions, and negative ions), $\bar{b}_E = \bar{B}_E/|\bar{B}_E|$ is defined as the unit vector in the direction of Earth's static magnetic field, $\omega_{pn} = \sqrt{\frac{q_n^2 N_n}{\varepsilon_0 m_n}}$ is the plasma frequency, $\omega_{Bn} = \frac{|q_n B_E|}{m_n}$ is the gyrofrequency, ν_n is the collision frequency, and $\bar{J}_{\text{tot}}$ is the total currents combining the contributions from every charge specie. Namely, $\bar{J}_{\text{tot}} = \sum_n \bar{J}_n$.

[12] For this specific application, equation (3) can be simplified for ease of implementation. First, since sprite initiation altitudes are below 90 km, where the electron-neutral and ion-neutral collision frequencies are much higher than lightning-generated electromagnetic wave frequencies, the first term on the left-hand side can be neglected. Second, because the sprites we investigated in this work occurred in the midlatitude regions where Earth's magnetic field is dominantly vertical, the cross term on the right-hand side can also be neglected with the minimum error. This approximation has been justified by our numerical experiments. However, for the applications where the higher altitude (above ~90 km) regions are involved in or the geomagnetic field is no longer vertical, this cross term has to be taken into account. According to equation (3), all of these charged particles affect lightning-generated electric fields in the ionosphere. However, these particles contribute to the electric fields to different degrees. At high altitudes, the effect of ions can be neglected because the mass of an ion is about 2000–6000 larger than an electron. On the other hand, at lower altitudes (below ~80 km), the positive ion density is higher than the electron density during nighttime. Consequently, the positive ions dominate the conductivity of the ionosphere at these altitudes and play a significant role in nighttime electromagnetic wave propagation.

[13] This model is a powerful tool to calculate electromagnetic fields generated by both lightning discharge currents and controlled sources. The frequency range of this model is broadened in comparison with previous models [*Ma et al.*, 1998; *Simpson and Taflove*, 2004]. We can easily include any ionosphere profiles, use arbitrary source current waveforms (provided they are cylindrically symmetric), and add horizontal medium inhomogeneity or Earth's magnetic field inhomogeneity in this model.

3.2. Lightning-Related Nonlinear Processes

[14] The original FDTD model developed by *Hu and Cummer* [2006] assumes the whole system to be linear and time-invariant. These two assumptions are correct in long distance (>200 km) propagation applications because the

disturbance of the ionosphere sometimes caused by big lightning discharges is localized [*Taranenko et al.*, 1993a] and the ionosphere is essentially stable on the timescale of lightning discharge processes. These two approximations are no longer correct in this particular application. In this work, we need to model the quasi-electrostatic fields right above the thunderclouds produced by the lightning discharges occurring below. These mesospheric electric fields above the thunderstorms caused by sprite-producing lightning discharges are intense enough to modify the ionosphere condition through some nonlinear processes, such as heating and ionization. To accurately model the electric fields above the thunderstorms for the purpose of the CB theory testing, we have to modify this two-dimensional cylindrical FDTD model by considering both heating and ionization processes, which lead to a substantial modification of the electron collision frequency and electron density at high altitudes (above ~60 km). On the other hand, the modified ionosphere condition above thunderstorms in turn affects the electric field. As a result, the whole system becomes a complicated nonlinear and time-variant system that can be solved by modifying the original FDTD model. We show below that including these effects in the model-data comparison is critically important.

[15] The heating process can be described by equation (4) [*Pasko et al.*, 1997a]:

$$\nu_e = \frac{q_e}{\mu_e m_e}, \tag{4}$$

where ν_e is the electron-neutral collision frequency, μ_e is the electron mobility, and m_e is the electron mass.

[16] The electron mobility is nonlinearly dependent on the electric fields through an empirical equation (5) [*Hegerberg and Reid*, 1980; *Davies*, 1983; *Pasko et al.*, 1997a]:

$$\begin{cases} \log(\mu_e N) = \sum_{i=0}^{2} a_i x^i, & EN_0/N \geq 1.62 \times 10^3 \text{ V/m} \\ \mu_e N = 1.36 N_0, & EN_0/N < 1.62 \times 10^3 \text{ V/m}. \end{cases} \tag{5}$$

where $x = \log(E / N)$, $a_0 = 50.970$, $a_1 = 3.026$, $a_2 = 8.4733 \times 10^{-2}$, N is the number density of air molecules, and N_0 is the number density of the air molecules at ground level. Observing equations (4) and (5), we notice that, when the magnitude of the electric field is small, the electron collision frequency remains the same as the ambient value and the heating effect is negligible. With the increase of the electric field, the heating effect becomes important and the electron mobility decreases. Thus, the electron collision frequency increases, the effective conductivity of the ionosphere is reduced, and the relaxation time of electric fields at high altitudes increases. Our numerical simulation indicates that the modification introduced by heating process affects the electric field distribution at high altitudes (above 60 km) significantly, which will be shown in section 4.1.

[17] Another nonlinear process, ionization, is described by equation (6) [*Pasko et al.*, 1997a]

$$\frac{dN_e}{dt} = (\nu_i - \nu_a) N_e. \tag{6}$$

[18] Here the ionization coefficient is defined as

$$\nu_i = 7.6 \times 10^{-13} N x^2 f(x) e^{-4.7(1/x-1)}, \tag{7}$$

where $f(x) = \frac{1+6.3e^{-2.6/x}}{1.5}$, $x = E / E_k$, and E_k is the characteristic air breakdown field [*Papadopoulos et al.*, 1993]. The attachment coefficient is defined in equations (8) and (9) [*Davies*, 1983; *Taranenko et al.*, 1993b]. When $EN_0 / N \geq 1.628 \times 10^6$ V/m,

$$\nu_a = \frac{N}{N_0} \sum_{i=0}^{2} a_i x, \tag{8}$$

where $x = EN_0 / N$, $a_0 = -2.41 \times 10^8$, $a^1 = 211.92$, and $a^2 = -3.545 \times 10^{-5}$. When $EN_0 / N < 1.628 \times 10^6$ V/m,

$$\log\left(\frac{\nu_a N_0}{N}\right) = \sum_{i=0}^{3} a_i x^i, \tag{9}$$

where $x = \log(EN_0 / N)$, $a_0 = 1073.8$, $a_1 = 465.99$, $a_2 = -66.867$, and $a_3 = 3.197$.

[19] According to the above equations, when the electric field is below the air breakdown threshold, the attachment process dominates the ionization process, which leads to a decrease of the electron density. Only if the electric field is above the air breakdown threshold, the ionization effect becomes dominant. In this work, we are mainly interested in the stages prior to sprite initiation, where the electric field is below the conventional breakdown threshold. Therefore the attachment effect dominates the ionization. Consequently, this process leads to a reduction of the electron density.

[20] In summary, the governing equations of this modified numerical model are equations (1), (2), and (3) and (4) and (6). The whole system is nonlinear and time-variant. Because the heating and ionization effects are only significant for electrons, we assume the ion densities and ion collision frequencies remain the ambient values.

[21] An assumption made in the above equations is that there is no energy and momentum relaxation time of the electron distribution needed for the energy distribution setup, which means the energy distribution is established instantaneously in response to a local electric field value. The energy and momentum relaxation time of the electron distribution increases with the altitude from 1–10 ps (ground level) to approximately 0.7 μs (~80 km above the ground), which is shorter than the timescale (2 μs) we used to evaluate the variation of the electric field in our FDTD model, therefore, we believe the error introduced by this assumption can be neglected, since in this particular application about sprite initiation, we are only interested in the altitudes around 80 km [*Liu and Pasko*, 2004].

3.3. Ionosphere Profiles

[22] In this work, three different ambient electron and ion density profiles, plotted in Figure 2, were employed to investigate the variability caused by the ionosphere uncertainty. The first electron density profile for altitudes above 80 km was obtained from the 2001 International Reference Ionosphere (IRI) model (http://modelweb.gsfc.nasa.gov/models/iri.html) with the following input parameters:

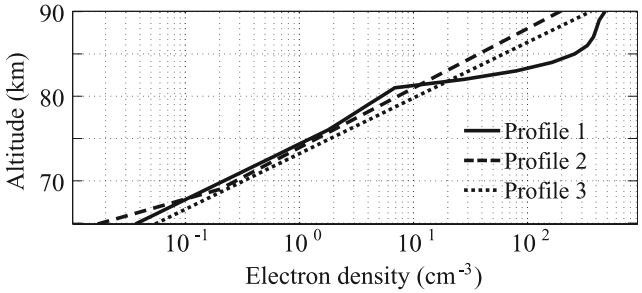

Figure 2. The nighttime electron density. Profile 1, calculated using 2001 IRI model; profile 2, taken from the work of *Pasko et al.* [1997a]; profile 3, inferred from the sferic data in July 2004 by using the ionosphere remote sensing technique.

41.9°N 98.4°W location, and 06:30 UT, 9 July 2004. The lower altitude (below 80 km) data of this profile are from the work of *Cummer and Inan* [2000]. The second electron density profile was adapted from the work of *Pasko et al.* [1997a]. The third electron density profile was calculated by [*Bickel et al.*, 1970; *Thomson*, 1993]:

$$N_e(h) = 1.43 \times 10^{13} \exp(-0.15h') \exp[(\beta - 0.15)(h - h')], \quad (10)$$

where $\beta = 0.5$ km^{-1} and $h' = 84.2$ km were inferred from the received sferic data during the nighttime on 15 July 2004, by using the ionosphere remote sensing system. *Bickel et al.* [1970] found that $\beta = 0.5$ km^{-1} and $h' = 85.5$ km are in good agreement with midlatitude nighttime observation, which are very close to the third profile we used here.

[23] As discussed earlier, the effect of ions, playing an important role in nighttime low frequency wave propagation, cannot be neglected here. Unfortunately, the knowledge about the *D* region ion species and concentrations is not thorough at all. As suggested by *Narcisi* [1971] and *Cummer and Inan* [2000], we set the positive ion density to be equal to the electron density except where N_e is below 100 cm^{-3}. For the altitudes where $N_e < 100$ cm^{-3}, we assume the positive ion density is equal to 100 cm^{-3}. The negative ion density is determined by the difference between the positive ion density and the electron density to maintain charge neutrality.

[24] The uncertainty of the model-predicted mesospheric electric fields introduced by the variation of the ionosphere profiles is dependent on altitudes. Below 65 km, the three ionosphere profiles result in almost the same electric field waveforms. For altitudes between 65 and 75 km, the disagreement among the simulated electric fields is noticeable but small. For altitudes above 75 km and below 83 km, the uncertainty is approximately within 20% at the time of the sprite initiation time. However, above 83 km, the uncertainty increases rapidly. Sprites are seldom triggered at very high altitudes since the intense electric fields cannot be sustained there due to the short relaxation time (our simulation results also validated this), therefore, in this work, we primarily focused on the regions below 83 km (because of the reasons stated above, this will not affect the conclusions of our analysis), where the ionosphere variability introduces a maximum uncertainty of 20% in model-predicted electric fields. In the following sections, we used the first profile in Figure 2 for the analysis.

[25] The ambient electron collision frequency was calculated using equations (4) and (5), where the number density of the air molecules was calculated using the Mass-Spectrometer-Incoherent-Scatter (MSIS-E-90) model (http://modelweb.gsfc.nasa.gov/models/msis.html). Again, the location we used is 41.9°N 98.4°W. The time input is 06:30 UT, 9 July 2004. Comparing this profile with the US Standard 1976 (http://www.pdas.com/atmos.htm), we find they are in good agreement because the largest discrepancy between these two profiles is less than ~10%, which occurs around 50 km. At 81 km, the altitude we are most interested in, the difference between them is only 4%. Furthermore, although a lower air number density means a lower E_k, the ratio E / E_k, the most important value we are concerned about in this work, may not change as significantly as E_k because a lower air density also implies a lower electron-neutral collision frequency and a higher conductivity, which leads to a lower electric field E. On the basis of our simulations, this air density uncertainty results in an error within 5% around 80 km at sprite initiation times, which is less than the ionospheric electron density uncertainty.

3.4. Source Modeling

[26] Unlike most of the previous models where a simple line source is assumed [*Hu and Cummer*, 2006], a more realistic source model was used for this work. This source model includes a horizontally extended structure of charged thunderclouds. The lightning return strokes are assumed to be an inward radial charge transfer from the whole charged region to the center of the region and then from the center to the ground. Consequently, there are not only vertical source currents but also azimuthally symmetric horizontal source currents inside this FDTD model. The radius of the charged disk is assumed to be 25 km. This ensures that the charge is removed from a horizontally extended region with the approximate area of 2000 km^2, which is in agreement with the observation of the sprite-producing positive lightning discharge [*Lyons et al.*, 2003].

[27] We have to mention that the area of the horizontal region where charges are removed affects the high-altitude electric fields significantly. According to our simulation results, if the charge region radius is extended from 25 to 50 km in our model, then the high-altitude (65–85 km) electric field amplitude drops by approximately 30% at the sprite initiation time for those sprites with very short (~2 ms) delays. On the other side, if we shrink the charge region from 25 km to a point charge, the corresponding high-altitude electric fields are only enhanced by 15%. Thus, readers should be reminded that the electric fields computed in this work are close to the maximum possible fields given a current moment waveform.

[28] The altitude of the positive charge layer, where the positive charge is transferred to ground during a sprite-producing lightning discharge, is assumed to be 6 km in this work consistent with measurements by *Marshall et al.* [2001] and *Lyons et al.* [2003]. Actually, because the region of interest in this work is high above the ground (>60 km), the lightning source altitude does not significantly affect the high-altitude electric fields. Our simulations results indicate

Figure 3. Images of typical S+, S, and S− sprite events: (a) S+, (b) S, (c) S−.

that, with a fixed current moment (the product of the electric current and the length of channel length), elevating the source region from the 6 to 8 km results in less than 3% variation in the electric fields above 60 km.

[29] With the features mentioned above, the lightning source modeling in this work is more realistic than other sources used in previous models [*Ma et al.*, 1998; *Hu and Cummer*, 2006].

4. Simulation Results and Analysis

[30] Optical emissions from the sprites were monitored on the video recordings at Yucca Ridge Field Station, Colorado. With the aid of National Lightning Detection Network (NLDN) data, we were able to select the sferic signals radiated by the corresponding sprite-producing lightning discharges from the data set continuously recorded by our ULF/ELF lightning remote sensing system. Only those signals with good signal-to-noise ratio (SNR) were picked for analysis to ensure the accuracy.

[31] According to CB theory, a sprite will be initiated when the lightning-generated quasi-electrostatic field exceeds the conventional breakdown threshold E_k, which is altitude dependent and can be calculated using $E_k = 3.2 \times 10^6\, N / N_0$ V/m, where $N_0 = 2.688 \times 1025\ \mathrm{m}^{-3}$ and N is the number density of the air molecules obtained using the MSIS-E-90 model. For ease of analysis, we defined a parameter termed normalized electric field $E_\mathrm{n} = E / E_k$, where E is the electric field produced by lightning discharges. With this definition, CB theory requires $E_\mathrm{n} > 1$ at some location for sprite initiation.

[32] The observed sprites were divided into three categories termed S+, S, and S− on the basis of their optical emission brightness. S are the sprites with the average brightness of those apparent events observed, S+ are unusually bright events (roughly upper 25%), and S− are dimmer events. Figure 3 shows the images of the typical sprite events representing these three categories. The standard for classifying these three categories is subjective but it provides a useful separation. We investigated these three categories separately to find how the sprite initiation condition is dependent on the intensity of sprites. We further divided the sprites into three different classes on the basis of their sferic signatures and their lightning-to-sprite delays. They are short-delayed ($\leq$25 ms) sprites with sprite currents, short delayed sprites without sprite currents, and long-delayed (>25 ms) sprites. For short delayed sprites, we can accurately infer the causative lightning discharge current moments using the deconvolution technique. For long-delayed sprites, which are often associated with long-lasting continuing lightning discharge currents, we use a different method for deriving the source currents because the deconvolution technique is unable to infer late time (>25 ms) source currents because of the frequency band limitation of our lightning remote sensing system. Sprites associated with sprite currents are especially important for our analysis. For this type of sprites, there is a second peak in the corresponding sferic waveform, which is temporally aligned with sprite brightness [*Cummer et al.*, 1998]. Hence the sprite initiation times of these sprites can be accurately determined (thus the electric fields upon the sprite initiation time can be accurately calculated) by observing the sferic waveforms. In the following subsections, we will analyze these event classes separately.

4.1. Short-Delayed Sprites With Sprite Current

[33] Some sferic waveforms contain ELF electromagnetic energy, which has been hypothesized to be radiated by the electric currents lasting from 2 to 4 ms flowing in the body of sprites [*Cummer et al.*, 1998; *Cummer and Stanley*, 1999; *Reising et al.*, 1999]. The temporal association between the ELF feature in the sferic waveforms and the sprite luminosity [*Cummer and Stanley*, 1999] enables us to determine the sprite initiation time with the minimal ambiguity. Observing the sferic waveforms of those sprites with sprite currents, we can easily find the accurate time of sprite initiation [*Hu et al.*, 2002] and thereby determine the magnitude of the quasi-electrostatic field as well as the associated charge moment changes at that specific time. Therefore sprites with sprite currents are very useful for the analysis of sprite initiation condition because it avoids the uncertainty of sprite initiation time determination imposed by the low time resolution of video.

[34] Most sprites associated with sprite currents are bright and classified as S+ events. Here we analyzed a bright sprite (S+) with a clear sprite current signature recorded on 9 July 2004 to test CB theory by incorporating our experimental data and numerical simulation results.

[35] This sprite event occurred at 06:26:07.6390 UT, 9 July 2004. The parent lightning discharge location is 41.9°N 98.4°W. The current moment inferred from the received sferic waveform is shown in Figure 4b. There is an evident second peak in the measurement inferred current moment waveform, which is believed to be contributed from the electric current flowing in the sprite body [*Cummer et al.*, 1998]. Because of the known relationship between the

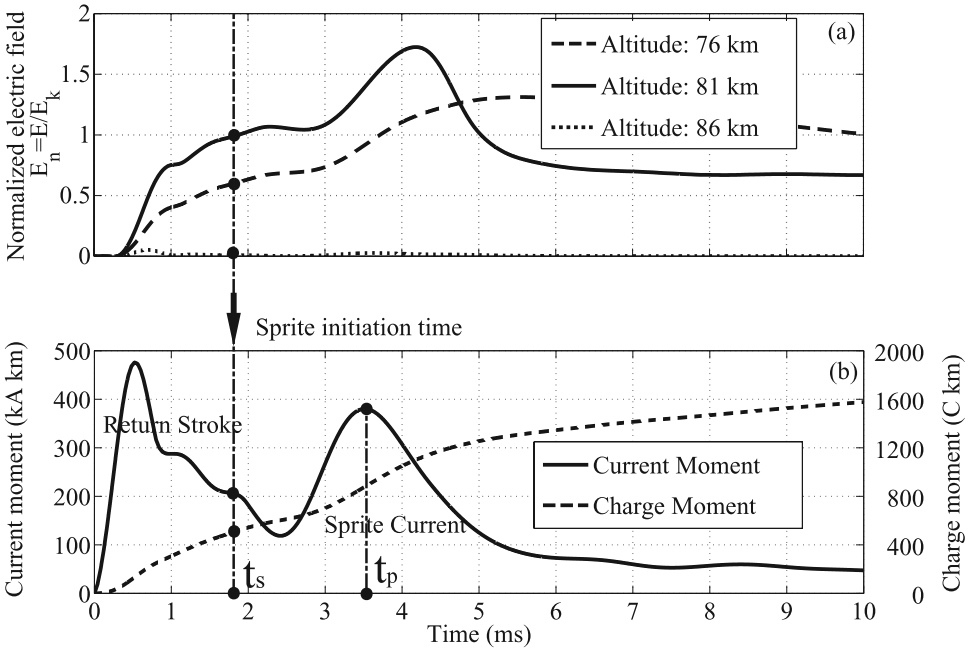

Figure 4. The CB sprite initiation theory testing on a short-delayed sprite with sprite current. (a) The simulated electric field waveforms above the thunderclouds; (b) the extracted current moment waveform of the parent lightning discharge and the corresponding charge moment change.

sprite luminosity and the radiated ELF energy from sprite currents (the second peak in the sferic waveform) [*Cummer et al.*, 1998], we can determine the time of the peak brightness of the sprite t_p accurately, as indicated in Figure 4b. In addition, the previous research using the high-speed video images has shown that the optical emissions were first visible about 1.0–2.5 ms before the peak sprite brightness [*Cummer and Stanley*, 1999]. Let these two times be $t_s^{\max} = t_p - 1.0$ ms and $t_s^{\min} = t_p - 2.5$ ms. Therefore, as a reasonable approximation, we can assume the sprite initiation time $t_s \approx \frac{1}{2}(t_s^{\min} + t_s^{\max})$. In this example, $t_p = 3.52$ ms; thus, $t_s^{\max} = 2.52$ ms, $t_s^{\min} = 1.02$ ms, and $t_s \approx 1.77$ ms, which is a little bit earlier than the detectable sprite current, as shown in the current waveform in Figure 4b.

[36] After inspecting the simulated electric field waveforms at various mesospheric altitudes carefully, we found that, at the time when the sprite was initiated ($t = t_s$), the peak normalized electric field was observed at 81 km. We plotted the modeled electric field waveform at 81 km in Figure 4a. The waveforms at 86 and 76 km are shown in the same figure for perspective. According to the simulation results in Figure 4a, the magnitude of the normalized electric field at 81 km $E_n^{81\ \mathrm{km}}(t_s) \approx 0.98$ ($E_n^{81\ \mathrm{km}}(t_s^{\min} < t < t_s^{\max}) \in [0.75, 1.07]$) while the normalized electric fields at 76 and 86 km are only 0.59 ($E_n^{76\mathrm{km}}(t_s^{\min} < t < t_s^{\max}) \in [0.41, 0.69]$) and 0.01 ($E_n^{86\ \mathrm{km}}(t_s^{\min} < t < t_s^{\max}) < 0.02$), respectively. At high altitudes above 81 km, the magnitude of the normalized electric field is smaller because the dielectric relaxation time decreases sharply with increasing altitude. At lower altitudes, the magnitude of the normalized electric field also gets smaller because the air breakdown threshold increases rapidly with decreasing altitude. At $t \approx t_s$, the maximum magnitude of the normalized electric field appeared at 81 km and the value is very close to 1, which implies that the model-predicted sprite initiation time based on CB theory is in excellent agreement with the experimentally observed sprite initiation time. In other words, the above analysis shows that the observed sprite was initiated at a time in complete agreement with CB theory.

[37] Figure 5 shows the effect of the heating and ionization processes at the optically observed sprite initiation time (1.77 ms after the return stroke). As shown in Figure 5a, below 90 km, the heating process affects the electron-neutral collision frequency significantly. The electron-neutral collision frequency at 81 km increases by a factor of 32. This enhancement of the electron-neutral collision frequency reduces the ionosphere conductivity at this altitude and eventually initiates a sprite. The ionization process also disturbs the ambient ionosphere condition but this effect is less important than the heating process in this event. At 81 km above the ground, the electron density is reduced to 30% at the sprite initiation time as shown in Figure 5b and this does not elevate the electric field at this altitude significantly based on our numerical simulation results. Combining the heating and ionization processes, we compared the resulting electric fields to the results without considering these processes in Figure 5c. Below 73 km, the nonlinear process has little effect on the electric fields (the E_n is enhanced from 0.40 to 0.42 at 73 km at the sprite initiation time if the nonlinear processes are taken into account). However, at altitudes around 81 km, the electric field is enhanced by a factor of 10 after including the nonlinear processes (from 0.093 to 0.98). Also, we plotted the conventional breakdown threshold E_k in Figure 5c for the reference.

[38] The model-predicted sprite initiation altitude as 81 km is generally in agreement with the previous optical observation results [*Stanley et al.*, 1999]. At low altitudes,

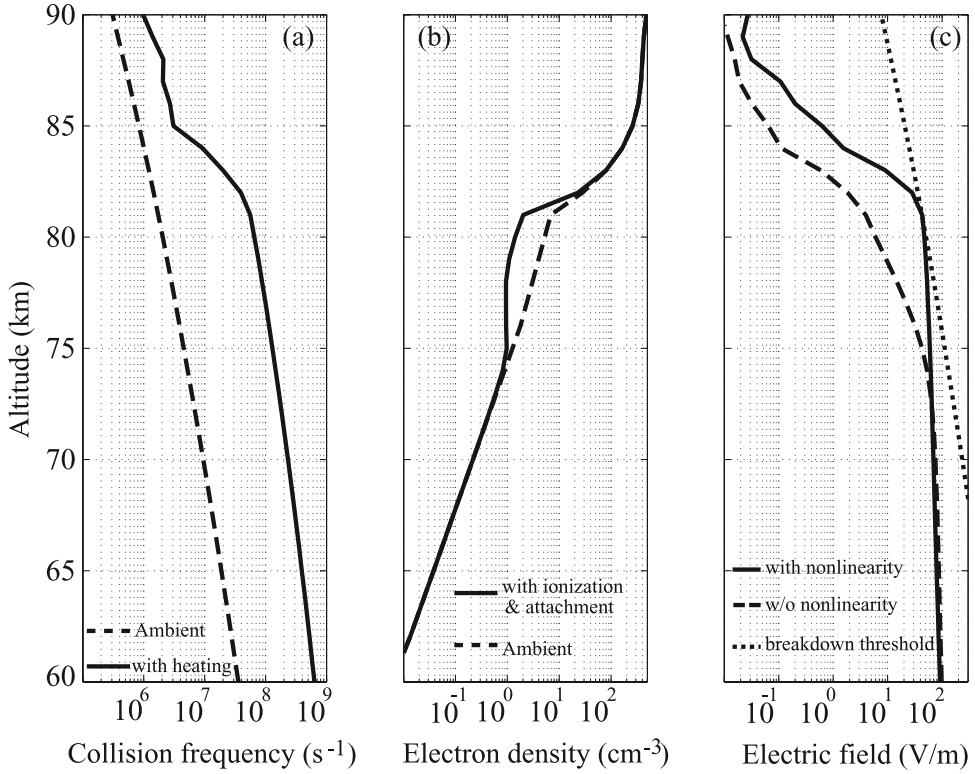

Figure 5. The effect of the heating and ionization processes on the collision frequencies, the electron densities, and the quasi-electrostatic fields above the thunderstorm at the model-predicted sprite initiation time (the sprite occurred at 06:26:07.6390 UT, 9 July 2004). (a) The ambient electron collision frequency and the electron collision frequency under the effect of the heating process; (b) the ambient electron density and the electron density under the effect of the ionization and attachment process; (c) the simulated electric field with the ambient ionosphere profile and the simulated electric field with the modified ionosphere by the heating and ionization processes.

the conventional breakdown threshold E_k is higher than that of high altitudes, thus the normalized electric field magnitude is smaller unless there is a continuing current in the causative lightning flowing between the cloud and ground sustaining the slowly decaying electric field. On the other hand, at high altitudes, the breakdown threshold E_k is small but the relaxation time is very short, thus the electric field at high altitudes attenuates rapidly. Therefore the normalized electric field at high altitude also cannot be very big unless the discharge current is very impulsive to set up the electric field quickly before it decays. Even in that case, the electric field cannot be sustained long enough to initiate a sprite based on simulations [*Pasko et al.*, 1999].

[39] The measurement-inferred charge moment change at the time of sprite initiation is approximately 500 C km, which is consistent with the previous measurements of charge moment changes for sprite initiation in sprite-producing lightning discharges [*Hu et al.*, 2002; *Cummer and Lyons*, 2005].

4.2. Short-Delayed Sprite Without Sprite Current

[40] We also investigated a number of short-delayed (<25 ms) sprites. First, we compute the quasi-electrostatic fields generated by the parent lightning discharges at the mesospheric altitudes. Then we estimated the sprite initiation times on the basis of the CB theory requirement ($E > E_k$). Finally, we compared the model-predicted sprite initiation times to the optical-observed sprite initiation times to see whether they are consistent to test CB theory.

[41] Most observed short-delayed sprites are not associated with sprite currents. For these sprites, we are unable to determine the sprite initiation time as accurately as those sprites with sprite currents. However, we can still determine a 16.7-ms-long time window [*Hu et al.*, 2002] of sprite initiation on the basis of the optical observations. Furthermore, because we know the precise times of the causative lightning return strokes using the NLDN data, this 16.7-ms-long time window can be narrowed down further for those sprites with the delay times shorter than 16.7 ms [*Hu et al.*, 2002]. For example, the optical observation at Yucca Ridge indicates there was a sprite (S+) initiated between 06:37:55.072 and 06:37:55.089 UT, 9 July 2004, and the parent lightning discharge of this sprite occurred at 06:37:55.078 UT, according to the NLDN data. Hence the sprite initiation time is within an 11-ms-long window (06:37:55.078 to 06:37:55.089) as shown in Figure 6b because sprites always occur after their parent lightning discharges. Here we call this time window the optical sprite initiation window (OSIW).

[42] We plotted the normalized electric field waveform E_n at 81 km in Figure 6a because it is the very first to across $E_n = 1$, which indicates that the sprite was initiated at this

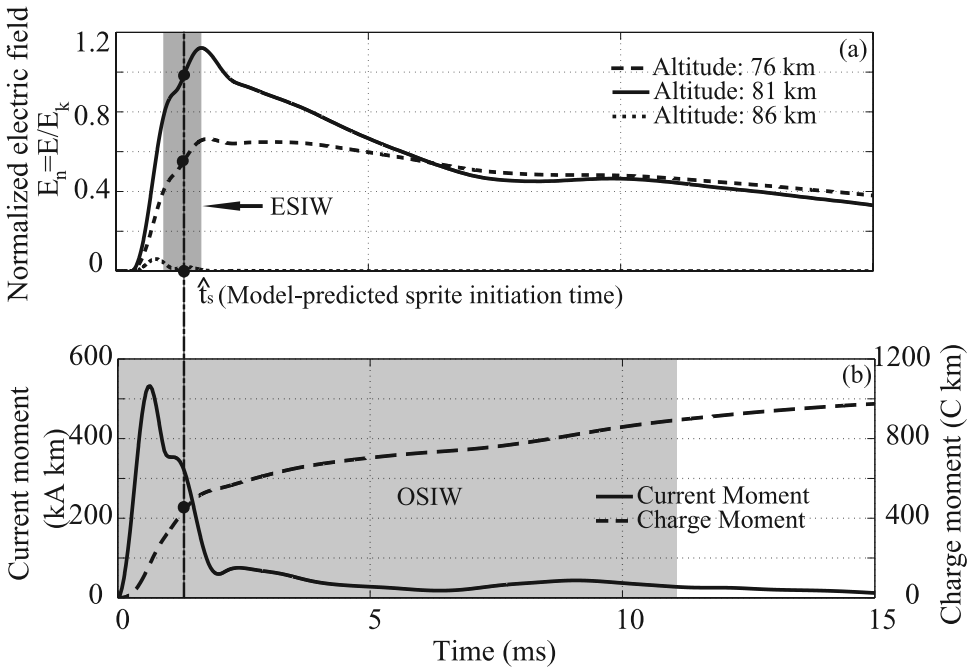

Figure 6. The CB theory testing on a short-delayed sprite without sprite current. The electrical sprite initiation window (ESIW) is defined by $t(E_n = 0.8) \leq t \leq \min[t(E_n = 1.2), t(E_n = \max(E_n))]$, and the optical sprite initiation window (OSIW) is the first video frame where the sprite is first visible in the optical sprite observation. (a) The simulated mesospheric electric field waveforms; (b) the measurement-inferred current moment waveform of the parent lightning discharge and the corresponding charge moment change.

altitude. Again, we plotted the electric fields at ±5-km altitudes for comparison. In consideration of the 20% variation in the modeled electric fields due to the electron density profile uncertainty, as a reasonable estimate, we define the estimate model-predicted sprite initiation time as

$$\hat{t}_s = \frac{t(E_n = 0.8) + \min[t(E_n = 1.2),\ t(E_n = \max(E_n)]}{2} \quad (11)$$

and define the time window $t(E_n = 0.8) \leq t \leq \min[t(E_n = 1.2), t(E_n = \max(E_n))]$ as the electrical sprite initiation window (ESIW). We notice the discharge in this event was quite impulsive and most charge was transferred to ground within the first 1.5 ms, which is shorter than the relaxation time at 80 km. Thus, the electric field increased rapidly in the first 1.5 ms after the return stroke and then attenuated slowly. Consequently, the ESIW is much narrower than the OSIW and the model-predicted sprite initiation time is well bounded. In this case, $\hat{t}_s \approx 1.3$ ms, which is within the optical observation window. This analysis again indicates that the numerical simulation results based on the measurement data are in agreement with CB theory. The charge moment change at the model-predicted sprite initiation time is 440 C km.

[43] We analyzed 15 short-delayed (<25 ms) sprites without sprite currents and shown the analysis results in Figure 7, where the long black bars represent the OSIW and the short gray bars represent the model-predicted sprite initiation times. The numbers inside the long black bars are the charge moment changes at the model-predicted sprite initiation times and those labeled with N/A mean that the mesospheric electric fields for those events are below the threshold for conventional breakdown (the numbers above those bars are the maximum normalized electric fields), and there is no model-predicted sprite initiation time can be found for those sprites. There are eight S+ events in this sprite set and seven of them have the model-predicted sprite initiation time within their OSIW, which again validated CB theory. However, six out of the seven dimmer sprite events (S and S−) in Figure 7 are associated with significantly lower normalized mesospheric electric fields. For these events, the measurement-inferred peak field is a factor of 2–8 lower than the threshold for conventional breakdown. It is unlikely that the ionosphere uncertainty and the measurement error (∼20%) cause this disagreement. Instead, it is possible that some other factors are playing an important role in the initiation of these sprites. For example, theoretical research suggests that gravity wave above mesoscale thunderstorms may modify the mesosphere density and facilitate a sprite [*Pasko et al.*, 1997b]. Meteoric dust particles could also participate in sprite initiation [*Zabotin and Wright*, 2001]. In addition, in this work, although we tried to pick those sprites produced by single lightning discharges, it is still possible that the preceding lightning discharges make significant contributions to the initiation of the sprites because the relaxation time for electron density enhancement in *D* region is usually much longer than the time period between consecutive lightning discharges [*Pasko et al.*, 1997a]. This means, the contributions from consecutive lightning discharges might accumulate and eventually initiate a sprite. However,

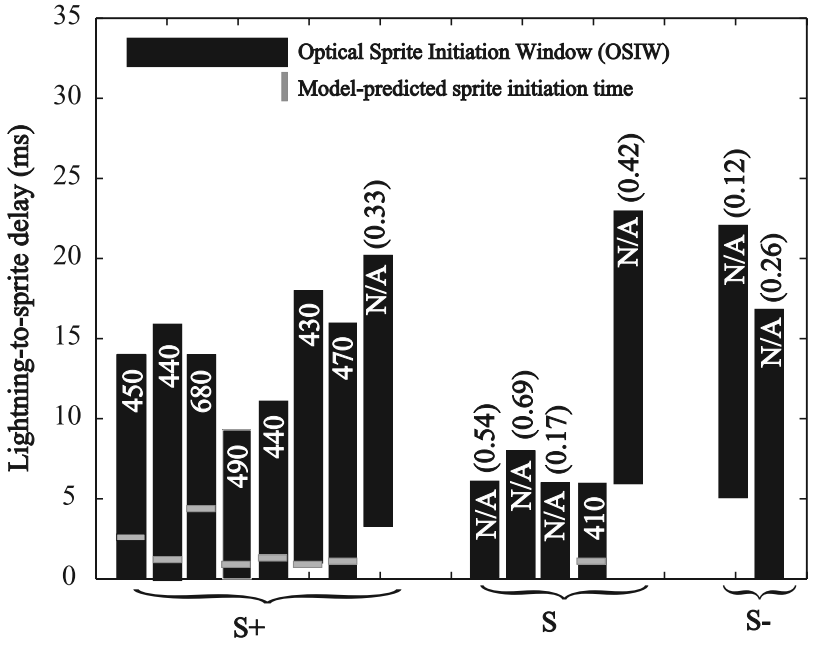

Figure 7. The CB theory testing results of short-delayed sprites without sprite current. The numbers in the long black bars are the charge moment change at the model-predicted sprite initiation time and the numbers above the bars are the maximum normalized quasi-electrostatic fields for those sprites whose simulated mesospheric electric fields were below the conventional breakdown threshold.

in this work, we only consider the effect from single lightning discharges. For further investigation of the disagreement between the optical measurements and the model prediction based on CB theory, high time resolution optical observation is needed to avoid the time uncertainty. The charge moment change at the sprite initiation time varies from 430 to 680 C km for the bright short-delayed sprite (S+) events. The average charge moment change is 490 C km. This value is consistent with the results of the statistical study of measured charge moment changes at sprite initiation times [*Hu et al.*, 2002] and is as accurate an estimate of this threshold as can be obtained without higher time resolution optical measurements.

4.3. Long-delayed sprites

[44] Previous studies show that intense continuing current in lightning moves a large amount of charge, and the total vertical charge moment change in the discharge can be enough to produce conventional breakdown in the mesosphere [*Cummer and Füllekrug*, 2001]. In this section, we quantitatively analyzed a sprite produced by a lightning with intense continuing current to find whether the conditions for sprite initiation according to CB theory are again satisfied for long-delayed sprite events. Usually, continuing currents are much weaker than lightning return strokes, which makes it difficult to infer continuing current waveforms accurately because of the low SNR. Therefore we picked those events with very intense continuing currents (thus the relative high SNR) for our analysis. Unfortunately, observing the sferic waveforms of these selected events, we usually find there were multiple lightning discharges detected between the causative lightning discharge and the sprite initiation, which complicates the analysis for the CB sprite initiation theory testing. Eventually, we only found one long-delayed sprite (S+) meeting the testing requirements, which occurred at 40.2°N 99.4°W, 06:42:41.0090 UT, 9 July 2004.

[45] The corresponding sferic waveform of this sprite in Figure 8c shows the elevated horizontal magnetic field after the return stroke, a clear signature of intense continuing current. In this case, we used a different approach to extract the lightning discharge current waveform. The source current here consists of two parts, the return stroke and the continuing current immediately following the return stroke. The former was calculated by the deconvolution method using the ELF sferic data. However, because the impulse response was experimentally determined by using the ELF data lacking low frequency (<100 Hz) components, we can only extract the current waveform with reasonable accuracy for about 25 ms because of the bandwidth limitation of the ELF remote sensing system. Assuming the continuing current is vertical and slowly varying, we can calculate the amplitude of the current using $I = 2\pi r h_i B_\phi / \mu_0 h_s$ as long as the receiver is far away from the lightning discharge [*Cummer and Füllekrug*, 2001], where h_i is the ionosphere height, h_s is the discharge channel length of the continuing current, B_ϕ is the measured horizontal magnetic field in distance, and r is the distance from the discharge to the receiver. The extracted current waveform is shown in Figure 8b.

[46] The optical sprite observation indicates that the sprite was initiated between 51 and 67 ms after the causative lightning return stroke, as shown in Figure 8b. In Figure 8a, we plotted the modeled electric field time waveforms at the altitude of 73 km because the normalized electric field at this altitude is higher than any other altitudes within the OSIW. The E_n at ±10 km are shown in the same plot for comparison. In this long-delayed sprite case, the maximum

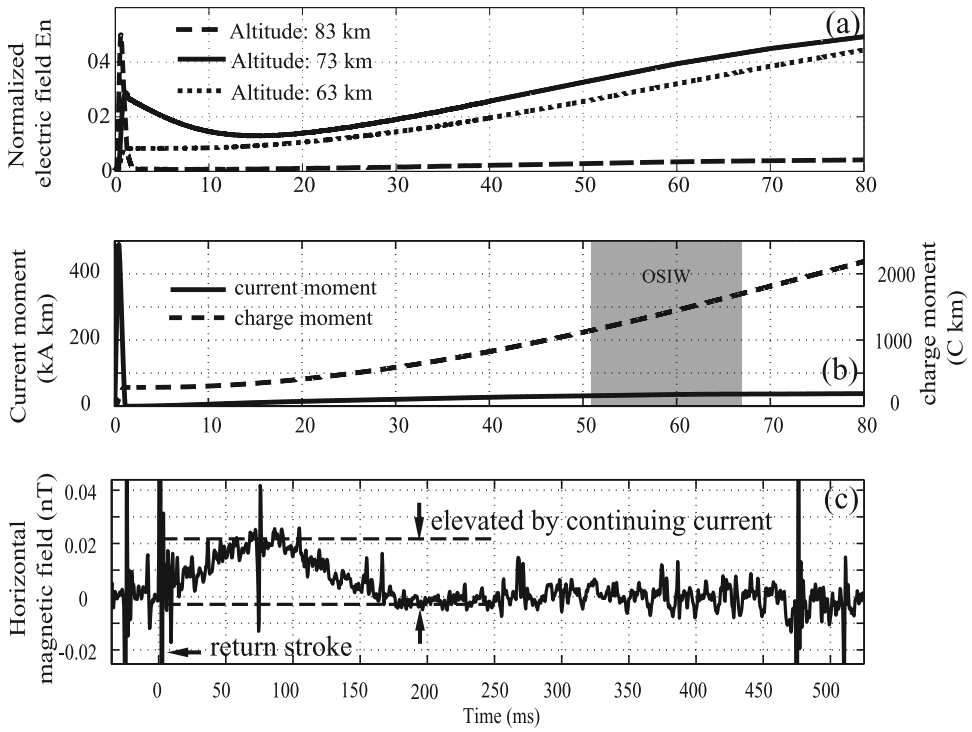

Figure 8. The CB theory testing on long-delayed sprite events produced by the intense continuing current. (a) The simulated electric fields above the thunderstorm; (b) the measurement-inferred current moment waveform and the charge moment change; (c) the observed sferic waveform at the receiver.

normalized electric field was observed at lower altitude than the short-delayed sprite initiation altitudes we just analyzed. This is reasonable because the relatively low rate of charge removal by the continuing current is unable to sustain the quasi-electrostatic field at high altitudes because of the short relaxation time there. However, the highest normalized electric field in the OSIW is lower than the threshold for conventional breakdown by a factor of 2 in this case, as was for the dimmer, short-delayed sprites. The origin of this factor of 2 or greater discrepancy merits further investigation but requires high time resolution optical measurements, which were not available in 2004.

[47] The measurement-inferred charge moment change at the sprite initiation time is between 1150 and 1700 C km, which is significantly larger than that for short-delayed sprites. This is not surprising because, for short-delayed sprites, the mesospheric electric field builds up quickly on a timescale of several milliseconds, which is shorter than the relaxation time. Although the charge transfer rate is very high for these short-delayed sprites, it lasts very shortly and the amount of the total charge removed is very limited. On the other hand, long-delayed sprites produced by continuing currents tend to occur at lower altitudes, where the relaxation time is longer and the air density is higher and hence the air breakdown threshold is higher. At these lower altitudes, the mesospheric electric field builds up relatively slowly because of the lower charge transfer rate from the cloud to the ground by the continuing current, and at the same time, the electric field decays because of the conductivity of the ionosphere. Consequently, long-delayed sprites need a larger charge moment change to sustain the mesospheric electric field until it exceeds the higher air breakdown threshold to initiate a sprite. This implies that there is no single charge moment change threshold for sprite initiation.

5. Conclusions and Discussions

[48] By combining the optical sprite observations, the recorded low frequency magnetic fields from lightning discharges, and a numerical full-wave FDTD model, we compared the inferred mesospheric electric field waveforms with the predictions of conventional breakdown theory. For bright, short-delayed sprite events, our analysis shows that the inferred mesospheric field at the sprite initiation time is within 20% of CB theory predictions. The full-wave nonlinear simulations suggest that sprite initiation altitude for short-delayed sprites is around 81 km. The model-predicted associated charge moment change for short-delayed sprite initiation varies from 430 to 680 C km with an average around 490 C km. This value is consistent with but more reliable than the previous measurements of charge moment changes for sprite initiation because the method we used in this work enables us to determine the sprite initiation time more accurately.

[49] This altitude is a little higher than the previous research on sprite initiation altitude observation [*Cummer and Stanley*, 1999; *Stanley et al.*, 1999; *McHarg et al.*, 2002]. We believe this discrepancy is reasonable for the following several reasons: (1) The model-predicted mesospheric electric field is dependent on the specific ambient

ionosphere profiles we use and the uncertainty of the ionosphere profile could lead to this kind of disagreement; (2) In this work, we define the model-predicted sprite initiation altitude as the altitude where the quasi-electrostatic field exceeds the conventional breakdown threshold earliest. However, $E > E_k$ does not guarantee a sprite generation. If the electric field cannot sustain long enough before the formation of streamers, then there is no sprite initiated at that altitude [*Pasko et al.*, 1999]. Therefore it is possible that sprites were initiated at lower altitudes even if the electric fields exceed E_k at higher altitudes first because of the shorter ionization time at lower altitudes. According to our simulation results, for the example shown in Figure 6, the electric field exceeds at E_k first at 81 km, but 0.2 ms later, the condition $E > E_k$ is satisfied 80 km. (3) The published sprite initiation altitudes were determined under the assumption that the sprites were directly over their parent lightning NLDN stroke locations. However, the lateral distance between sprites and their parent strokes can be up to 50 km [*Lyons*, 1996], which leads to an uncertainty in sprite altitude as high as 10 km [*Cummer and Stanley*, 1999; *Stanley et al.*, 1999; *McHarg et al.*, 2002].

[50] For dimmer sprites (S or S−) and long-delayed sprite events, the measurement-inferred electric field at the time of sprite initiation is consistently a factor of 2–8 smaller than CB theory predictions. This suggests that there might be some other mechanisms that enhance the mesospheric electric field locally in these cases. Further investigation is warranted and will require high time resolution optical measurements to give sprite initiation times with approximately 1 ms precision.

[51] **Acknowledgments.** The Duke University component of this research was supported by NSF Aeronomy Program grant ATM-0436585. The FMA Research component of this work was partially supported by NSF grant ATM-0221512. We thank Victor Pasko for his illuminating comments and his suggestion to include the nonlinear processes in our numerical model.

References

Bell, T. F., V. P. Pasko, and U. S. Inan (1995), Runaway electrons as a source red sprites in the mesosphere, *Geophys. Res. Lett.*, *22*(16), 2127–2130, doi:10.1029/95GL02239.

Bell, T. F., S. C. Reising, and U. S. Inan (1998), Intense continuing currents following positive cloud-to-ground lightning associated with red sprites, *Geophys. Res. Lett.*, *25*(8), 1285–1288, doi:10.1029/98GL00734.

Bickel, J. E., J. A. Ferguson, and G. V. Stanley (1970), Experimental observation of magnetic field effects on VLF propagation at night, *Radio Sci.*, *5*, 19.

Cummer, S. A., and U. S. Inan (1997), Measurement of charge transfer in sprite-producing lightning using ELF radio atmospherics, *Geophys. Res. Lett.*, *24*(14), 1731–1734, doi:10.1029/97GL51791.

Cummer, S. A., U. S. Inan, T. F. Bell, and C. P. Barrington-Leigh (1998), ELF radiation produced by electrical currents in sprites, *Geophys. Res. Lett.*, *25*(8), 1281–1284, doi:10.1029/98GL50937.

Cummer, S. A., and M. Stanley (1999), Submillisecond resolution lightning currents and sprite development: Observations and implications, *Geophys. Res. Lett.*, *26*(20), 3205–3208, doi:10.1029/1999GL003635.

Cummer, S. A., and U. S. Inan (2000), Modeling ELF radio atmospheric propagation and extracting lightning currents from ELF observations, *Radio Sci.*, *35*(2), 385–394, doi:10.1029/1999RS002184.

Cummer, S. A. (2000), Modeling electromagnetic propagation in the Earth-ionosphere waveguide, *IEEE Trans. Antennas Propag.*, *48*, 1420–1429.

Cummer, S. A., and M. Füllekrug (2001), Unusually intense continuing current in lightning produces delayed mesospheric breakdown, *Geophys. Res. Lett.*, *28*(3), 495–498, doi:10.1029/2000GL012214.

Cummer, S. A., and W. A. Lyons (2005), Implications of lightning charge moment changes for sprite initiation, *J. Geophys. Res.*, *110*, A04304, doi:10.1029/2004JA010812.

Davies, D. K. (1983), Measurements of swarm parameters in dry air, Theoretical Notes, Note 346, Westinghouse R&D Center, Pittsburgh, Pa.

Gerken, E. A., U. S. Inan, and C. P. Barrington-Leigh (2000), Telescopic imaging of sprites, *Geophys. Res. Lett.*, *27*(17), 2637–2640, doi:10.1029/2000GL000035.

Hegerberg, R., and I. D. Reid (1980), Electron drift velocities in air, *Aust. J. Phys.*, *33*, 227.

Hu, W., S. A. Cummer, W. A. Lyons, and T. E. Nelson (2002), Lightning charge moment changes for the initiation of sprites, *Geophys. Res. Lett.*, *29*(8), 1279, doi:10.1029/2001GL014593.

Hu, W., and S. A. Cummer (2006), An FDTD model for low and high altitude lightning generated EM fields, *IEEE Trans. Antennas Propag.*, *54*(5), 1513–1522.

Lehtinen, N. G., T. F. Bell, V. P. Pasko, and U. S. Inan (1997), A two-dimensional model of runaway electron beams driven by quasi-electrostatic thundercloud fields, *Geophys. Res. Lett.*, *24*(21), 2639–2642, doi:10.1029/97GL52738.

Lehtinen, N. G., U. S. Inan, and T. F. Bell (2001), Effects of thunderstorm-driven runaway electrons in the conjugate hemisphere: Purple sprites, ionization enhancements, and gamma rays, *J. Geophys. Res.*, *106*(A12), 28841–28856, doi:10.1029/2000JA000160.

Liu, N., and V. P. Pasko (2004), Effects of photoionization on propagation and branching of positive and negative streamer in sprites, *J. Geophys. Res.*, *109*, A04301, doi:10.1029/2003JA010064.

Lyons, W. A. (1996), Sprite observations above the U.S. high plains in relation to their parent thunderstorm systems, *J. Geophys. Res.*, *101*(D23), 29,641–29,652.

Lyons, W. A., T. E. Nelson, E. R. Williams, S. A. Cummer, and M. A. Stanley (2003), Characteristics of sprite-producing positive cloud-to-ground lightning during the 19 July STEPS mesoscale convective systems, *Mon. Weather Rev.*, *131*, 2417–2427.

Ma, Z., C. L. Croskey, and L. C. Hale (1998), The electrodynamic responses of the atmosphere and ionosphere to the lightning discharge, *J. Atmos. Terr. Phys.*, *60*, 845–861.

Marshall, T. C., M. Stolzenburg, W. D. Rust, E. R. Williams, and R. Boldi (2001), Positive charge in the stratiform cloud of a mesoscale convective system, *J. Geophys. Res.*, *106*(D1), 1157–1164, doi:10.1029/2000JD900625.

McHarg, M. G., R. K. Haaland, D. Moudry, and H. C. Stenbaek-Nielsen (2002), Altitude-time development of sprites, *J. Geophys. Res.*, *107*(A11), 1364, doi:10.1029/2001JA000283.

Narcisi, R. S. (1971), Composition studies of the lower ionosphere, in *Physics of the Upper Atmosphere*, edited by F. Verniani, Editrice Compositori, Bologna, Italy. Reproduced in Handbook of Geophysics and the Space Environment, S. Adolph Jursa, Ed., Air Force Geophysics Laboratory, Air Force Systems Command, Air Force, U.S., Springfield, VA, 1985, 21-56.

Papadopoulos, K., G. Milikh, A. Gurevich, A. Drobot, and R. Shanny (1993), Ionization rates for atmospheric and ionospheric breakdown, *J. Geophys. Res.*, *98*(A10), 17593–17596, doi:10.1029/93JA00795.

Pasko, V. P., U. S. Inan, T. F. Bell, and Y. N. Taranenko (1997a), Sprites produced by quasi-electrostatic heating and ionization in the lower ionosphere, *J. Geophys. Res.*, *102*(A3), 4529–4562, doi:10.1029/96JA03528.

Pasko, V. P., U. S. Inan, and T. F. Bell (1997b), Sprite as evidence of vertical gravity wave structures above mesoscale thunderstorms, *Geophys. Res. Lett.*, *24*(14), 1735–1738, doi:10.1029/97GL01607.

Pasko, V. P., U. S. Inan, and T. F. Bell (1998), Spatial structure of sprites, *Geophys. Res. Lett.*, *25*(12), 2123–2126, doi:10.1029/98GL01242.

Pasko, V. P., U. S. Inan, and T. F. Bell (1999), Mesospheric electric field transients due to tropospheric lightning discharges, *Geophys. Res. Lett.*, *26*(9), 1247–1250, doi:10.1029/1999GL900240.

Raizer, Y. P., G. M. Milikh, M. N. Shneider, and S. V. Novakovski (1998), Long streamers in the upper atmosphere above thunder cloud, *J. Phys. D: Appl. Phys.*, *31*, 3255–3264.

Reising, S. C., U. S. Inan, and T. F. Bell (1999), ELF sferic energy as proxy indicator for sprite occurrence, *Geophys. Res. Lett.*, *26*(7), 987–990, doi:10.1029/1999GL900123.

Roussel-Dupré, R., and A. V. Gurevich (1996), On runaway breakdown and upward propagating discharges, *J. Geophys. Res.*, *101*(A2), 2297–2312, doi:10.1029/95JA03278.

Simpson, J., and A. Taflove (2004), Three-dimensional FDTD modeling of impulsive ELF propagation about the Earth-ionosphere, *IEEE Trans. Antennas Propag.*, *52*(2), 443–451.

Stanley, M., P. Krehbiel, M. Brook, C. Moore, W. Rison, and B. Abrahams (1999), High speed video of initial sprite development, *Geophys. Res. Lett.*, *26*(20), 3201–3204, doi:10.1029/1999GL010673.

Taranenko, Y., and R. Roussel-Dupre (1996), High altitude discharges and gamma-ray flashes: A manifestation of runaway air breakdown, *Geophys. Res. Lett.*, *23*(5), 571–574, doi:10.1029/95GL03502676.

Taranenko, Y. N., U. S. Inan, and T. F. Bell (1993a), Interaction with the lower ionosphere of electromagnetic pulses from lightning: Heating,

attachment, and ionization, *Geophys. Res. Lett.*, *20*(15), 1539–1542, doi:10.1029/93GL01696.

Taranenko, Y. N., U. S. Inan, and T. F. Bell (1993b), The interaction with the lower ionosphere of electromagnetic pulses from lightning: Excitation of optical-emissions, *Geophys. Res. Lett.*, *20*(23), 2675–2678, doi:10.1029/93GL02838.

Thomas, J. N., R. H. Holzworth, M. P. McCarthy, and O. Pinto Jr. (2005), Predicting lightning-driven quasi-electrostatic fields at sprite altitudes using in situ measurements and a numerical model, *Geophys. Res. Lett.*, *32*, L10809, doi:10.1029/2005GL022693.

Thomson, N. R. (1993), Experimental daytime VLF ionospheric parameters, *J. Atmos. Terr. Phys.*, *55*, 173–184.

Yukhimuk, V., R. A. Roussel-Dupré, and E. M. D. Symbalisty (1999), On the temporal evolution of red sprites: Runaway theory versus data, *Geophys. Res. Lett.*, *26*(6), 679–682, doi:10.1029/1999GL900073.

Zabotin, N. A., and J. W. Wright (2001), Role of meteoric dust in sprite formation, *Geophys. Res. Lett.*, *28*(13), 2593–2596, doi:10.1029/2000GL012699.

S. A. Cummer, Department of Electrical and Computer Engineering, Duke University, Durham, NC, USA.

W. A. Lyons, Forensic Meteorology Associates, Research, Fort Collins, CO, USA.

W. Hu, Schlumberger-Doll Research, One Hampshire Street, Cambridge, MA 02139, USA. (whu@boston.oilfield.slb.com)